Polymer 275 (2023) 125915

Contents lists available at ScienceDirect

Polymer

journal homepage: www.elsevier.com/locate/polymer

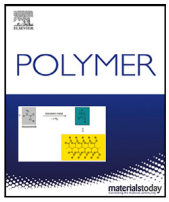

Surface properties of μm and sub-μm polydimethylsiloxane thin films after oxygen plasma treatment

Yijie Xiang *, Bozhidar Dejkoski, Paul Fulmek, Ulrich Schmid

Institute of Sensor and Actuator Systems, TU Wien, Gusshausstrasse 27-29, E366 02, Vienna, 1040, Vienna, Austria

ARTICLE INFO

Keywords:
PDMS
Wettability
Hydrophobic recovery
Oxygen plasma treatment
Buckling structure

ABSTRACT

Polydimethylsiloxane (PDMS) is widely used in many areas of science due to its outstanding properties. The continuous expansion of its applications is evidenced by a large number of research studies dedicated to modifying this soft material, ultimately leading to tailored properties. These studies highlighted the important role of film thickness (in the range of a few micrometers to millimeters) on surface properties, including mechanical properties, wettability, and surface topography. In this work, we investigated these surface properties of pristine as well as oxygen plasma-treated PDMS, in a thickness range of submicrometer and micrometer. We explored the effects of film thickness, dilution ratio, and plasma treatment time on effective Young's modulus, surface topography (buckling structures), and wettability (hydrophobicity recovery) of the PDMS surfaces by conducting force–distance measurements, atomic force microscopy (AFM) and contact angle (CA) measurements, respectively, over a period of more than one month after the plasma treatment. The results of effective Young's modulus on pristine PDMS show a high correlation with the dilution ratio and no dependency on the thickness. The characterized waviness (λ) and amplitude (A) of the resulting buckling structures forming on the plasma-treated surfaces reveal a correlation with film thickness, which is not included in the theoretical predictions. The results of CAs show a faster recovery process for the advancing than for the receding condition, and uncover a high correlation with both film thickness and dilution ratio for short-time plasma treatment. Furthermore, the buckling structures as well as the hydrophobicity recovery process in this work revealed a significantly different domain in comparison to the studies in literature, where these properties of PDMS membranes with a thickness ranging from a few micrometers to a few millimeters have been investigated.

1. Introduction

Polydimethylsiloxane (PDMS) exhibits excellent thermal and chemical stability, optical transparency, biocompatibility, and extreme cost-efficiency, and offers possibilities for efficient modification of its mechanical properties [1–3], wetting characteristics [4–6], and surface topography [1,3,7]. These unique properties continuously attract considerable interest and attention, leading to various application areas such as surface engineering [8–11], optical gratings [12,13], microfluidics [14–16], stretchable electronics [17], biochips [10,15,18] and so on.

The surface wetting property of PDMS, described by water contact angle (CA), can be efficiently modified from hydrophobic to hydrophilic using oxygen plasma or UV/ozone (UVO) treatment by introducing silanol (Si-OH) terminal groups and generating a silica layer on the surface [1–5,7,15,19]. Moreover, the hydrophobicity recovers over time due to the reorientation of the hydrophilic terminal groups into the bulk material and the penetration of low molecule weight (LMW) species from bulk to the surface [15]. In addition to the wettability modification, the oxygen plasma treatment can also modify the surface topography of PDMS. The plasma introduces high energy to the surface and drastically increases the surface temperature. Compressive stress is created in the stiff silica layer on the soft PDMS during the cooling process. As the compressive stress reaches a critical value, buckling structures are formed to relieve the stress [6,19–22].

The continuous expansion of PDMS's application domain is evidenced by a large number of research studies dedicated to modifying this soft material, ultimately leading to tailored properties that cater to specific purposes and applications. For instance, Pascual et al. [23] proposed a method to locally tune the wettability of a PDMS surface. This method involves local heating of a plasma-hydrophilized PDMS

* Corresponding author.
E-mail addresses: yijie.xiang@tuwien.ac.at (Y. Xiang), bozhidar.dejkoski@tuwien.ac.at (B. Dejkoski), paul.fulmek@tuwien.ac.at (P. Fulmek), ulrich.e366.schmid@tuwien.ac.at (U. Schmid).

https://doi.org/10.1016/j.polymer.2023.125915
Received 1 February 2023; Received in revised form 27 March 2023; Accepted 29 March 2023
Available online 3 April 2023
0032-3861/© 2023 The Authors. Published by Elsevier Ltd. This is an open access article under the CC BY license (http://creativecommons.org/licenses/by/4.0/).

Table 1
The dilution ratio, thickness, and effective surface near Young's modulus for each sample type. Buckling structures are formed on the surface after 15 and 30 s oxygen plasma treatment. The characterized waviness (λ) and amplitude (A) of the buckling structures on each sample are shown in this table as well.

Sample	Ratio [wt%]	Thickness [μm]	E [MPa]	λ [nm]		A [nm]	
				15 s	30 s	15 s	30 s
M	0:1	3.5 ± 0.10	3.1 ± 0.12	222 ± 0.1	231 ± 9.2	6.3 ± 0.63	19.8 ± 1.87
m	5:1	3.5 ± 0.10	1.8 ± 0.19	321 ± 14.1	342 ± 2.1	17.5 ± 1.22	27.0 ± 3.14
N	5:1	0.86 ± 0.13	1.8 ± 0.14	299 ± 7.8	318 ± 12.0	14.4 ± 1.79	23.6 ± 2.45
n	9:1	0.86 ± 0.13	0.9 ± 0.06	380 ± 41.7	367 ± 13.44	16.1 ± 1.74	31.7 ± 3.12

surface to accelerate the hydrophobicity recovery process while the rest surface remains hydrophilic [23]. Tan et al. [13] proposed tunable phase gratings by wrinkling of the plasma-oxidized PDMS [13]. Additionally, a few review papers are available for the various applications and modifications of PDMS in recent years [10,15,16,24,25]. Despite its significance and application interest, the surface properties of pristine and plasma-treated PDMS are subject to variability due to the influence of fabrication parameters (e.g. prepolymer-to-crosslinker ratio, treatment time) as well as the layer thickness [1–5,26,27]. Liu et al. [2] investigated the mechanical properties of PDMS with a thickness ranging from 30 to 350 μm and the results showed that an increased thickness results in a decrease in Young's modulus [2]. Hyun and Jeong [1] deposited a thin polymer layer on an oxygen plasma-treated PDMS surface and induced buckling structures on the surface. The resulting waviness of the buckling structures (2.76, 3.31 and 3.52 μm) increases when the thickness of PDMS increases (0.5, 2 and 20 mm) [1]. Nguyen et al. [4] and Bhandaru et al. [5] investigated the effect of thickness on the hydrophobicity recovery process after hydrophilization of the PDMS surface, in the thickness range of a few micrometers to one millimeter and 3.9 to 30 mm, respectively. Both studies revealed a faster recovery process on thicker films [4,5]. Firpo et al. [28] showed that the permeability of PDMS membranes to CO_2 and He depends on the membranes thickness below tens of micrometers [28]. In summary, these studies highlight the critical role of the PDMS film thickness on the mechanical properties, the resulting buckling structures, hydrophobicity recovery after surface modification, and consequently the applications of PDMS. As PDMS films become progressively thinner in many device applications, it is crucial to understand how surface properties of PDMS in the micrometer and submicrometer thickness range depend on process parameters.

In this work, we manage to provide a comprehensive understanding of the surface properties of both pristine and plasma-modified PDMS thin films in the thickness range of submicrometer and micrometer. We fabricated thin PDMS films by varying the dilution ratio, exposed the PDMS surface to oxygen plasma treatment with various treatment times, and investigated a wide range of surface properties, namely, effective Young's modulus, surface topography, and wetting properties as well as the hydrophobicity recovery process, over a time period of more than one month.

2. Experimental details

2.1. Materials and sample preparation

The PDMS elastomer was prepared by mixing the prepolymer base and the crosslinker with a 10:1 ratio by weight (Sylgard 184 kit, Dow Corning). Next, it was degassed in a vacuum desiccator for 30 min. To achieve film thicknesses in the micrometer and sub-micrometer range, the PDMS mixture was diluted with a non-aqueous liquid, n-heptane, at various dilution ratios. The diluted PDMS mixture was spin-coated onto a silicon die with a dimension of 20 × 20 mm^2 in a nitrogen environment. The spin coating process was carefully optimized by adjusting the spin speed and time [15,29]. Subsequently, the samples were cured for 2 h at 100 °C in a clean room environment. The thickness of the films was determined by measuring the step height with a profilometer (Dektak). The dilution ratio, i.e., n-heptane to PDMS by mass, and the resulting thickness for each sample are shown in Table 1. For a better overview in the following part, the PDMS films with a thickness of 3.5 μm and 0.86 μm are labeled *M*, *m* (indicating the micrometer range) and *N*, *n* (indicating the nanometer range), respectively. A lowercase letter, for instance, *m*, indicates a relatively higher dilution ratio than the uppercase letter, *M*. The applied spin speed and spin time for achieving the desired thickness are 7000, 500, 6000, and 500 rpm and 150, 30, 120, and 30 s for sample *M*, *m*, *N*, and *n*, respectively.

The oxygen plasma treatment of the PDMS films was conducted in an STS 320 RIE plasma etching system using a radio frequency (RF) power supply at 13.56 MHz. The plasma chamber was firstly evacuated to a pressure of 12 mTorr and purged by nitrogen gas. The oxygen plasma treatment was then conducted at a chamber pressure of 20 mTorr, oxygen gas flow rate of 20 sccm, plasma power of 100 W, and various treatment times: 5, 15 and 30 s, followed by a purging process through nitrogen gas for 1 min and pumping down the pressure back to 12 mTorr for 2 min. In the following chapter, the number after each sample labeling represents the treatment time, e.g. *N5* for an *N* sample treated by oxygen plasma for 5 s. The samples were stored in ultra-violet (UV) light protected boxes in a clean room.

2.2. Characterization

The surface topography was analyzed with an atomic force microscope (AFM, Bruker Dimension Edge, cantilever NCHV-A). Based on the AFM results, the characteristic waviness and amplitude of the buckling structure were acquired by Gwyddion [30]. The former one is quantified by the height–height correlation function [31]. Additionally, effective Young's modulus was obtained based on the force–distance curves measured through the contact mode of AFM [29,32–34]. The cantilever applied for contact mode is the Bruker Scanasyst-Fluid with a spring constant of 0.7 N/m. Typical acquired force–distance curves are shown in Fig. 1. These force–distance curves were then used for effective Young's modulus determination by the open-source software AtomicJ [34,35], which supports a wide range of contact mechanics models for various materials, including the hyperelastic PDMS. The measurement of the force–distance curve was repeated at three different positions for each sample. The arithmetic mean value is then presented for effective Young's modulus in the following sections.

A drop shape analyzer (DSA, Krüss DSA30S) with a resolution of 0.01° and an accuracy of 0.1°, was used for the contact angle (CA) measurement. The wettability of samples is described by the advancing and receding water CA through the sessile drop method [36,37] at laboratory atmospheric condition with a temperature of 20 ± 1 °C and humidity of 35 ± 5 %. The advancing CA was measured by increasing the droplet volume through the dosing needle [37]. As the receding CA is considerably smaller (<20 °) and even zero (see results and discussion part of wettability), it was impossible to use the same dosing system to establish the receding CA. Therefore, we applied the droplet evaporation method [38–40] to measure the receding CA. The maximum speed of the volume change for advancing and receding CA was 0.1 μL/s and 0.003 μL/s, respectively. The volume change results in a triple line movement. The capillary number, Ca, is used to evaluate the effect of the triple line movement on the determination of contact

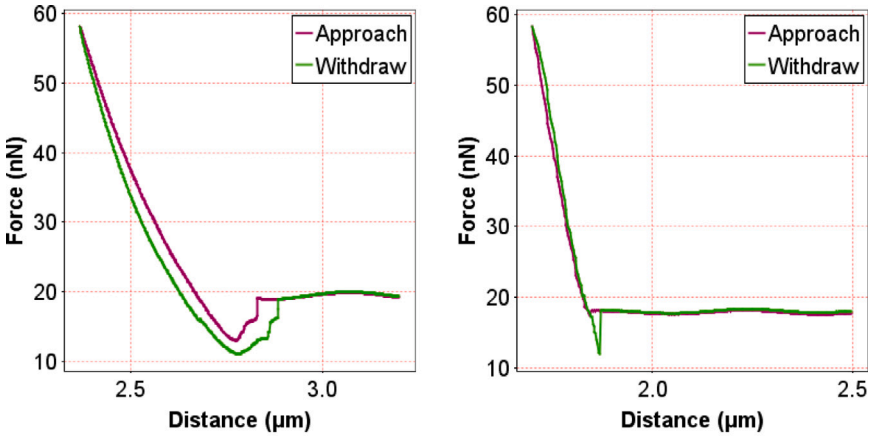

Fig. 1. The force–distance curve acquired by AFM for (a) untreated pristine sample *n*, and (b) *m* sample treated by oxygen plasma for 15 s, *m15*.

angle. Ca is calculated by $Ca = (\mu \cdot v)/\gamma_{la}$, with dynamic viscosity μ, liquid–air surface tension γ_{la} and triple line velocity v, and describes the relative effect of viscous drag force versus surface tension [41]. The maximum Ca due to the triple line movement, which is induced by volume change in this work, is equal to $7.2 \cdot 10^{-6}$. This value is smaller than the critical value of $\approx 10^{-5}$. Therefore, in the first approximation, the effect of viscous forces on the CA can be neglected [36,41,42], and we may say that the triple line movement and volume change do not play a role in the CA determination.

3. Results and discussion

3.1. Effective Young's modulus

The obtained results of the effective Young's modulus of each sample are shown in Table 1. The value for cross-linked PDMS film with a dilution ratio of 0:1 (*M* sample, non-diluted), 3.1 ± 0.12 MPa, is comparable to those in literature [1,15,43,44]. The samples *m* and *N*, which have the same dilution ratio (5:1) but with different film thicknesses, show an identical value of effective Young's modulus. We may therefore conclude that the dilution ratio plays the dominant role in the effective Young's modulus of the film in the investigated thickness range, as only a higher dilution ratio results in a lower value of effective Young's modulus.

There are a few studies in the literature investigating Young's modulus of cross-linked PDMS films and membranes [1–3,45]. The work of Liu et al. [2], who fabricated PDMS membranes in a thickness range of 35–350 μm from non-diluted PDMS, revealed a thickness-dependency of Young's modulus [2]. An increase in thickness leads to a decrease in Young's modulus of the cross-linked PDMS. This result is in contrast to ours, as the effective surface near Young's modulus appeared independent of the film thickness, in the investigated thickness of 0.86 μm and 3.5 μm. In addition to the thickness difference, it is necessary to note that in their study, the tensile tests were performed by a microforce tester for acquiring Young's modulus, indicating the property of the bulk material, while in our work, the force–distance curves were conducted by AFM, revealing the surface near Young's modulus. Hyun and Jeong [1] and Kim et al. [3] investigated the effect of prepolymer-to-crosslinker ratio on Young's modulus of bulk PDMS [1,3]. Their results revealed that a lower prepolymer-to-crosslinker ratio (higher percentage of crosslinker) leads to a higher density of crosslinked PDMS and therefore a higher Young's modulus. In our investigations, the prepolymer-to-crosslinker ratio is kept at 10:1 and the mixture of prepolymer and crosslinker is diluted by n-heptane to achieve thin layers by spin-coating. Our results provide new insight into controlling the effective surface near Young's modulus.

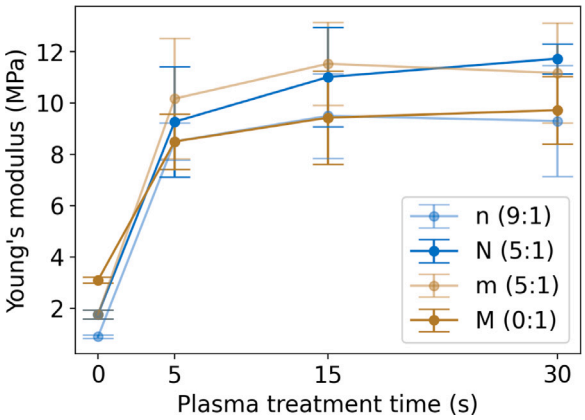

Fig. 2. The effective surface near Young's modulus of PDMS as a function of plasma treatment time.

Recent work from Inoue et al. [45], who diluted the PDMS with hexane to create PDMS rubber and conducted tensile tests, showed a similar dependence of bulk Young's modulus on the dilution ratio.

After the formation of the stiff silica layer on the surface by oxygen plasma treatment, the effective surface near Young's modulus increased to 8–10 MPa, as shown in Fig. 2. When the plasma treatment time increases, the value of the effective surface near Young's modulus is slightly enhanced. No clear correlation can be seen between effective Young's modulus and sample type (i.e. PDMS film thickness and dilution ratio).

The effective surface near Young's modulus has been investigated over time. The results reveal a decrease smaller than 1 MPa on all types of samples over one month. It is important to note that the thickness of the silica layer generated by plasma treatment is in the range of a few nanometers [46], and the effective Young's modulus measured by force–distance curve refers to the bilayer, i.e., the silica/PDMS layer.

3.2. Surface topography

In the following the results of surface topography analyses with respect to the plasma treatment time, the sample type (thickness, dilution ratio, and effective Young's modulus) and as a function of time are discussed.

To start, the results of surface topography changing with plasma treatment times are presented and discussed. Examples of AFM images of both untreated and plasma-treated *N* samples are shown in Fig. 3.

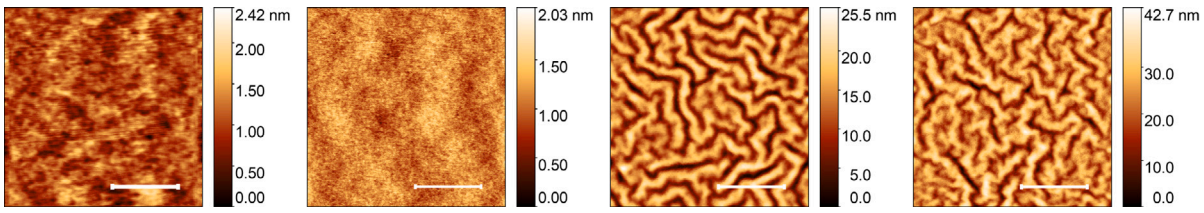

(a) *N* (b) *N5* (c) *N15* (d) *N30*

Fig. 3. Topography of *N* samples (dilution ratio of 5:1) for (a) non-treated surface; treated by oxygen plasma for (b) 5 s, (c) 15 s, and (d) 30 s. The length of the white bar represents 1 μm.

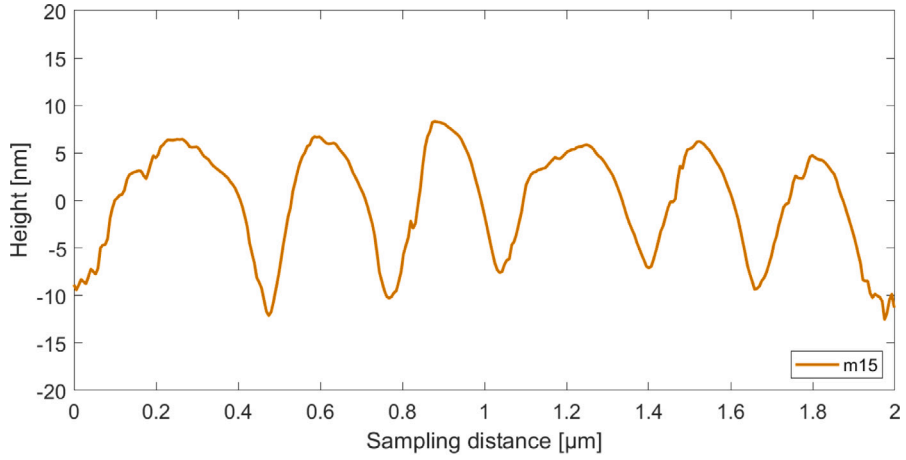

(a)

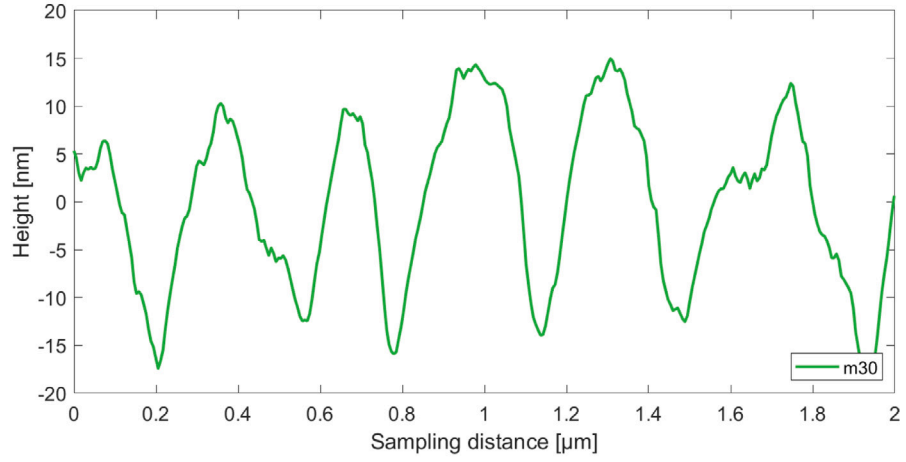

(b)

Fig. 4. Typical surface profiles for sample *m* treated by oxygen plasma for 15 s (a) and 30 s (b).

At a treatment time of 5 s, the surface topography stays unchanged compared to the pristine PDMS surface, while the CAs show a dramatic drop (for details see Discussion of wetting property). This dramatic drop in CAs indicates that the oxygen plasma treatment introduces the hydrophilic silanol (Si-OH) terminal groups and generates a silica layer [15]. A significant topographical modification is observed after 15 s plasma treatment, as buckling structures are formed on the surface, see Fig. 3(c). This surface modification is due to the mismatch of the thermal expansion coefficients of the stiff silica surface (1×10^{-6} K^{-1} to 1×10^{-7} K^{-1}) and the bulk elastomeric PDMS ($\approx 3.1 \times 10^{-4}$ K^{-1}) [6,20–22]. The plasma treatment considerably increases the sample temperature while the stiff silica layer is generated. Compressive stress is created in the top silica layer when the temperature decreases again during the purging process. The buckling structures are therefore formed to relieve the compressive stress [6,20–22], as we can see from the AFM images illustrated in Fig. 3(c)(d). Typically, the buckling structure is characterized by its waviness λ and amplitude A, which are described by [19,47,48]

$$\lambda = 2\pi h_s \left(\frac{\overline{E}_s}{3\overline{E}_P} \right)^{1/3}, \tag{1}$$

and

$$A = h_s \left(\frac{\varepsilon}{\varepsilon_c} - 1 \right)^{1/2}, \tag{2}$$

where h_s is the thickness of the stiff silica layer. $\overline{E}_s$ and $\overline{E}_P$ are the in-plane strain moduli of the silica and PDMS layer, and are described by

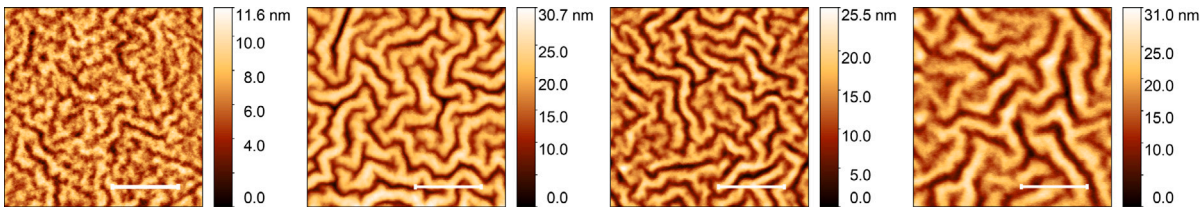

(a) *M15 (0:1)* (b) *m15 (5:1)* (c) *N15 (5:1)* (d) *n15 (9:1)*

Fig. 5. AFM images of all samples after plasma treatment for 15 s. The length of the white bar represents 1 μm.

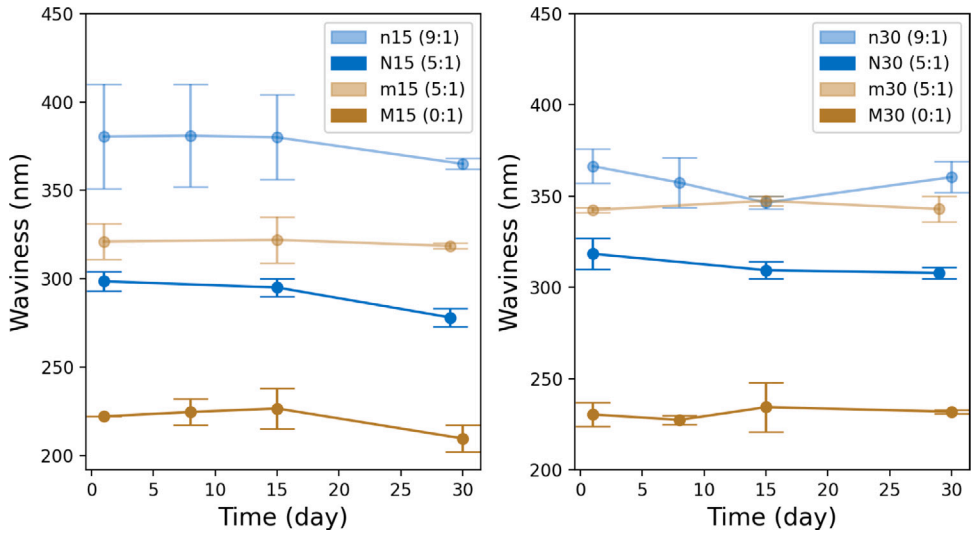

Fig. 6. The time dependency of the waviness of the buckling structure after oxygen plasma treatment for 15 s (left) and 30 s (right). Day 0 represents the day of the plasma treatment. The surface topography investigation was started on day 1 to eliminate the impact of the surface free radicals generated by plasma treatment on the results. The number after the sample's labeling refers to the plasma treatment time in seconds. The ratio in brackets is the dilution ratio.

Young's modulus E and Poisson's ratio ν, as $\overline{E} = E/(1-\nu^2)$. ε represents the compressive strain on the bilayer. The parameter ε_c is described by

$$\varepsilon_c = \frac{1}{4}\left(\frac{3\overline{E}_P}{\overline{E}_s}\right)^{2/3}, \tag{3}$$

and defined as the critical buckling strain, or in other words, the minimum strain needed to induce buckling [48]. These equations indicate that the waviness and amplitude are both proportional to the thickness of the silica layer, and the latter additionally depends on the strain.

The results of waviness and amplitude for the buckling structure are shown in Table 1, and reveal enhanced values of both on samples *M*, *m*, and *N*, when the plasma treatment time increases from 15 to 30 s. This increasing trend of waviness and amplitude with plasma treatment time is consistent with Eqs. (1) and (2). As the plasma treatment time increases, the thickness of the silica layer (h_s) and the thermally-induced strain (ε) raises [49–51]. The raise in the former (h_s) results in an increase in waviness, while the raise of both the h_s and ε leads to an increase in amplitude. Accordingly, the amplitude shows a more pronounced increase (>50%) compared to waviness (<7%). Typical surface profiles of the *m* sample treated for 15 and 30 s are shown in Fig. 4 and reveal the significant increase in amplitude with plasma treatment time. However, the waviness of sample *n* shows a higher deviation in comparison to other samples. The waviness changes from 380 ± 41.7 to 367 ± 13.44. No significant increasing trend of waviness by increasing the plasma treatment time can be revealed, as the error bars overlap.

Additionally, the surface topography is discussed regarding the sample type, more specifically, thickness, dilution ratio, and effective Young's modulus. We assume that the thickness of the silica layer is independent of the sample type, as it is determined by the plasma treatment time and energy input [49–51]. According to Eq. (1), a decreased value of Young's modulus of PDMS leads to a raised value in waviness. Our results are consistent with this statement, see the waviness results in Table 1, and AFM images in Fig. 5. Furthermore, by comparing the samples *m* and *N*, which have the same dilution ratio (5:1) and effective Young's modulus of PDMS (1.8 MPa), but different thicknesses, the waviness of the buckling structure on sample *m* (3.5 μm), is larger than on sample *N* (0.86 μm). It is evident that the thickness of the PDMS also plays a role in waviness. This correlation between the PDMS thickness and the waviness is not included in Eq. (1).

The resulting amplitude shows a similar trend as the waviness. The higher the effective Young's modulus, the higher the critical strain ($\varepsilon_c \propto \overline{E}_P^{2/3}$), and accordingly, the lower the amplitude of the resulting buckling structure, as described by Eq. (2). In addition to the effective Young's modulus, the thickness of the PDMS layer also contributes to the resulting amplitude. The thicker the PDMS film, the larger the amplitude of the formed buckling structure. This correlation between the amplitude and the film thickness is also not included in Eq. (2).

Moreover, the surface topography has been investigated over a period of 30 days after plasma treatment. The waviness and amplitude of the buckling structure as a function of time are shown in Figs. 6 and 7, respectively. The blue graphs represent results for the sub-micrometer samples *N* and *n*, while the brown graphs show results for the micrometer samples, *M* and *m*. The lighter color represents samples with a higher dilution ratio. The results reveal a rather constant waviness and a decrease in amplitude over time, and the latter indicates surface relaxation.

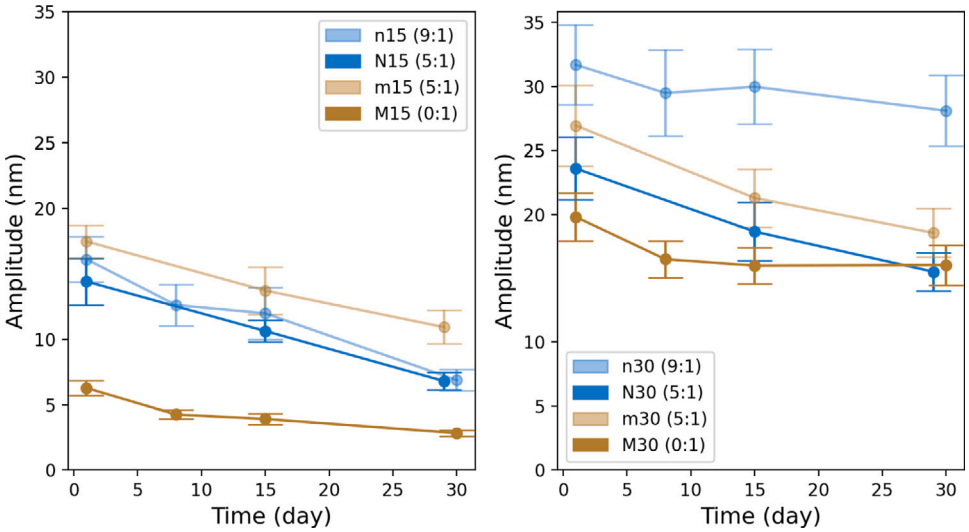

Fig. 7. The time dependency of the amplitude of the buckling structure after oxygen plasma treatment for 15 s (left) and 30 s (right).

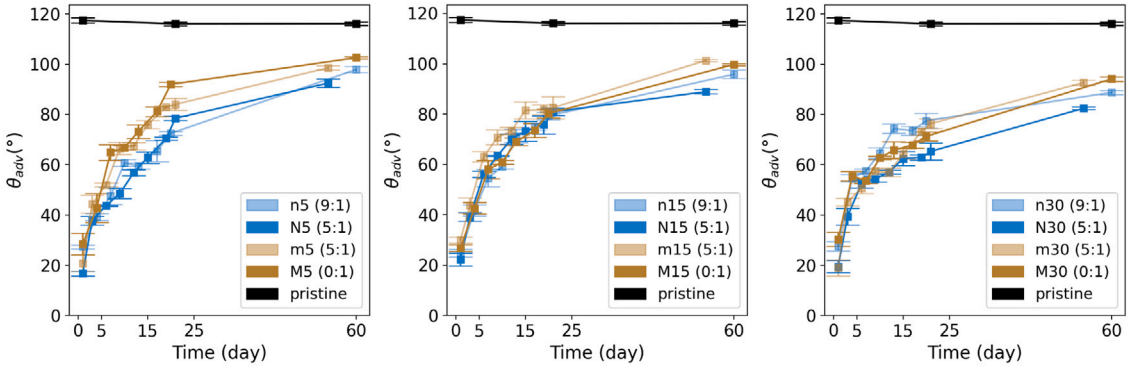

(a) advancing limit

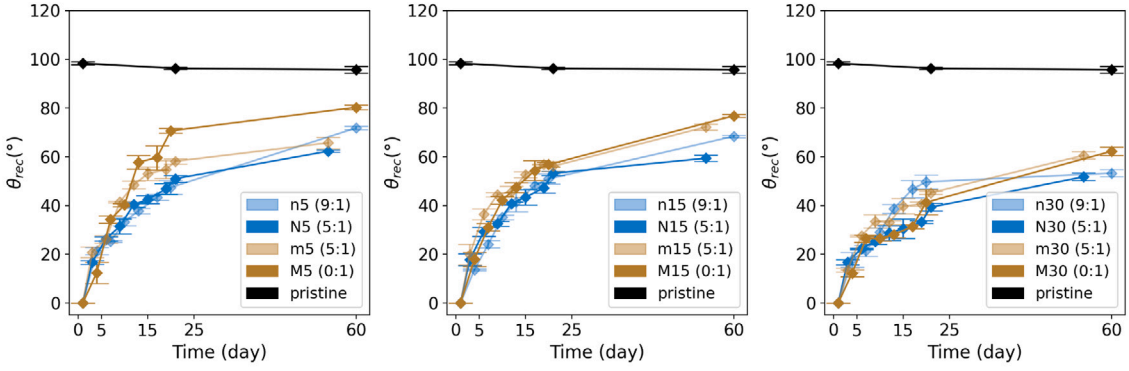

(b) receding limit

Fig. 8. Time dependent advancing (a) and receding CA (b). The CAs on pristine (untreated samples), θ_p, are shown in black. The hydrophobicity recovery process is shown by the CA raise on the plasma-treated surfaces over time. From left to right: PDMS treated by oxygen plasma for 5, 15, and 30 s.

3.3. Wetting property

The CA results are shown in Fig. 8. The advancing and receding CA on pristine PDMS, $\theta_p^{adv} = 117.4 \pm 1.02°$ and $\theta_p^{rec} = 98.4 \pm 0.61°$, reveal its natural hydrophobicity. The CAs drastically reduce to a hydrophilic state by the oxygen plasma treatment. These initial CAs on plasma-treated PDMS, $\theta_i^{adv} = 17–27°$ and $\theta_i^{rec} = 0°$, as shown in Fig. 8 at the first day after plasma treatment, are independent of the plasma treatment time, surface topography, film thickness, and dilution ratio. This reduction of CAs is attributed to the creation of hydrophilic silanol (Si-OH) terminal groups on the surface [4,5,15]. The CAs on these plasma-treated surfaces increase over time due to the reorientation of the hydrophilic functional groups to the bulk PDMS and the migration of hydrophobic LMW species from bulk to the surface [4,5,15]. Fig. 8 depicts the recovery process as the CAs on plasma-treated surfaces increase with time.

According to Young's equation [52], the CA is determined by the force equilibrium of the surface tensions at the triple line. This allows

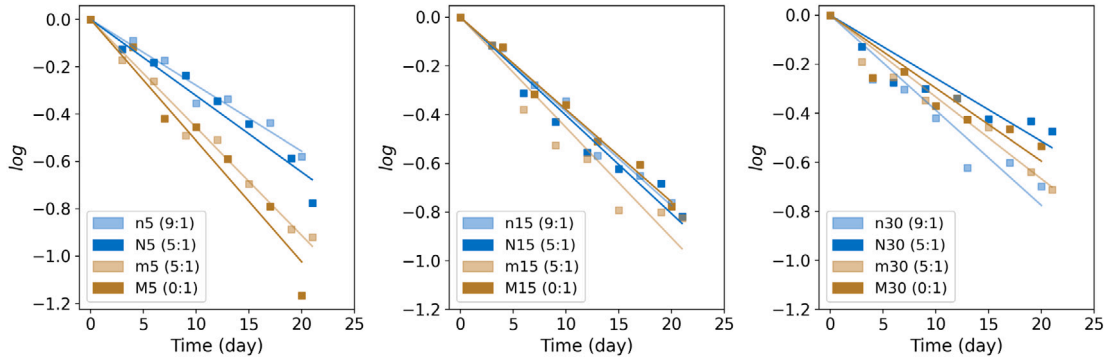

(a) advancing limit

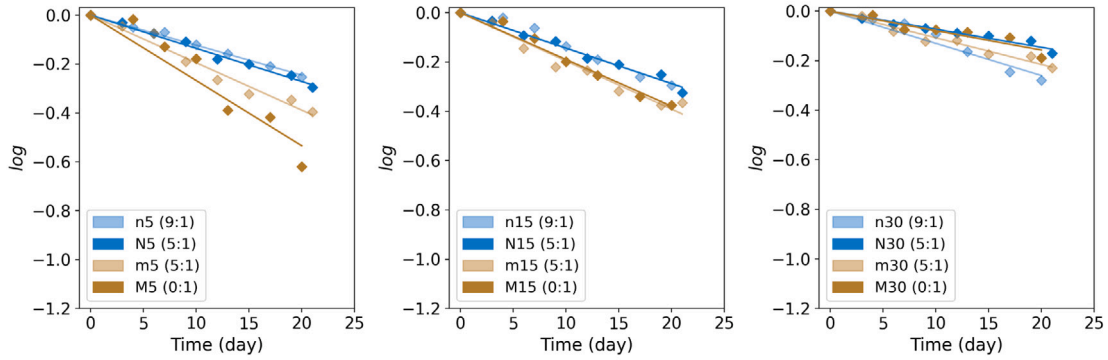

(b) receding limit

Fig. 9. Results of $\log(\frac{\gamma-\gamma_p}{\gamma_i-\gamma_p})$ at the (a) advancing limit and (b) receding limit. The inserted lines represent the linear fit. The recovery speed in the first recovery stage is represented by the absolute value of the slope, $1/\tau$.

the effective solid surface tension, γ, to be expressed as

$$\gamma = \gamma_{sa} - \gamma_{sl} = \gamma_{la}\cos(\theta), \tag{4}$$

where the γ_{sa}, γ_{sl} and γ_{la} represent solid–air, solid–liquid and liquid–air interface tension. θ can be advancing or receding CA. Using the measured CAs and the γ_{la} at 20 °C, 72.8 mN/m[53], the effective solid surface tension, γ, is calculated for the advancing and receding limit.

In order to characterize the recovery process, we approximate the recovery process by an exponential function, starting with the effective solid surface tension of the initial plasma-treated surface, γ_i, and assume that the final state of the recovery process is the pristine PDMS, γ_p. The recovery process of hydrophobicity described by γ is therefore written as

$$\gamma = (\gamma_i - \gamma_p)\cdot\exp(-\frac{t}{\tau}) + \gamma_p, \tag{5}$$

where τ is the time constant and characterizes the initial and maximum speed of the recovery process. γ_i and γ_p are calculated through Eq. (4) with the corresponding θ_i and θ_p, respectively.

The recovery process within the first month is fitted according to Eq. (5). The slope of the fitting line, $-1/\tau$, is shown in Fig. 9, and characterizes the recovery speed. The higher the $1/\tau$, the faster the surface hydrophobicity recovers. Overall, the recovery speed reveals a smaller value when the plasma treatment time increases, and shows a significantly smaller value in the receding limit than in the advancing limit. For PDMS treated by oxygen plasma for 5 s, the recovery speed ($1/\tau$) for the micrometer samples *M* and *m* is considerably larger than that for the sub-micrometer samples *N* and *n*. Additionally, the dilution ratio contributes to the recovery process as well. A lower dilution ratio leads to a higher recovery speed. This higher recovery speed is assumed to be caused by the greater reservoir of LMW species in the thicker [4,5,15] and the less-diluted PDMS films. However, for samples treated with oxygen plasma for 15 and 30 s, there is no clear correlation between recovery speed and film thickness or dilution ratio. It is worthwhile to mention that we have neglected the influence of the buckling structures on the CAs, since the effective increase of the surface area by the buckling structures is less than 4.4%. The CAs were measured again two months after the plasma treatment as shown in Fig. 8. The CAs on all plasma-treated samples did not reach the hydrophobic state of pristine PDMS.

4. Conclusion

In this work, we explored the effects of film thickness (submicrometer and a few micrometers), dilution ratio, and plasma treatment time on effective Young's modulus, wettability, hydrophobic recovery, and buckling structure of PDMS surfaces.

The results of effective Young's modulus on pristine PDMS show a high correlation with the dilution ratio and are independent of thickness. A higher dilution ratio leads to a lower effective Young's modulus of PDMS. The oxygen plasma treatment can modify both surface wettability and surface topography. The hydrophilization of the PDMS does not depend on the film thickness, dilution ratio, and oxygen plasma treatment time. Even a 5-second oxygen plasma treatment results in a significant drop in CAs. However, the hydrophobicity recovery process does show a dependency on both film thickness and dilution ratio. Thicker and less-diluted PDMS films lead to a higher recovery speed due to their higher LMW species reservoirs. Moreover, the recovery speed shows a lower value as the treatment time increases, and reveals a higher value in the advancing than in the receding limit.

Surface topography is modified, namely, buckling structures are formed on the surface when the critical strain is reached, in our case, when the plasma treatment time is longer than 15 s. Our results reveal

that the thickness of PDMS has an impact on both waviness and amplitude. A higher thickness results in higher values of both. Furthermore, the buckling structure has been observed over time, the results show a constant value of the waviness but a decrease in amplitude.

All in all, the surface properties of PDMS can be easily and efficiently modified by oxygen plasma treatment, and the resulting properties highly depend on the dilution ratio and film thickness. In comparison to thicker PDMS films (ranging from a few tens of micrometers to millimeters), thin films (submicrometer and micrometer range) exhibit significantly different domains of buckling structures and hydrophobicity recovery. The buckling structures forming on thin films exhibit a waviness in the submicrometer range, while thicker films typically show a waviness ranging from a few micrometers to tens of micrometers. Moreover, the recovery process of hydrophobicity for thin films is considerably longer, lasting more than a month, in contrast to thicker films which typically recover within a few days or even hours. These differences in the surface properties underscore the impact of film thickness, indicating that the film thickness is crucial for advancing the proper utilization of PDMS in various applications.

CRediT authorship contribution statement

Yijie Xiang: Conceptualization, Formal analysis, Validation, Visualization, Writing – original draft. **Bozhidar Dejkoski:** Investigation, Data curation, Validation, Visualization, Writing – review & editing. **Paul Fulmek:** Validation, Writing – review & editing. **Ulrich Schmid:** Supervision; Writing – review & editing.

Declaration of competing interest

The authors declare the following financial interests/personal relationships which may be considered as potential competing interests: Ulrich Schmid reports financial support was provided by the Austrian Research Promotion Agency (FFG).

Data availability

Data will be made available on request.

Acknowledgments

This work was funded by the FFG "Produktion der Zukunft" program under grant agreement number 871392. This support is gratefully acknowledged.

References

[1] D.C. Hyun, U. Jeong, Substrate thickness: An effective control parameter for polymer thin film buckling on PDMS substrates, J. Appl. Polym. Sci. 112 (5) (2009) 2683–2690.
[2] M. Liu, J. Sun, Y. Sun, C. Bock, Q. Chen, Thickness-dependent mechanical properties of polydimethylsiloxane membranes, J. Micromech. Microeng. 19 (3) (2009) 035028.
[3] E.S. Kim, S.H. Kim, S.-J. Lee, J.H. Lee, M. Byeon, D.H. Suh, W.J. Choi, Facile fabrication of micro/nano-structured wrinkles by controlling elastic properties of polydimethylsiloxane substrates, Polymer 212 (2021) 123087.
[4] L. Nguyen, M. Hang, W. Wang, Y. Tian, L. Wang, T.J. McCarthy, W. Chen, Simple and improved approaches to long-lasting, hydrophilic silicones derived from commercially available precursors, ACS Appl. Mater. Interfaces 6 (24) (2014) 22876–22883.
[5] N. Bhandaru, N. Agrawal, M. Banik, R. Mukherjee, A. Sharma, Hydrophobic recovery of cross-linked polydimethylsiloxane films and its consequence in soft nano patterning, Bull. Mater. Sci. 43 (1) (2020) 1–10.
[6] A. Tserepi, E. Gogolides, K. Tsougeni, V. Constantoudis, E.S. Valamontes, Tailoring the surface topography and wetting properties of oxygen-plasma treated polydimethylsiloxane, J. Appl. Phys. 98 (11) (2005) 113502.
[7] A. Chiche, C.M. Stafford, J.T. Cabral, Complex micropatterning of periodic structures on elastomeric surfaces, Soft Matter 4 (12) (2008) 2360–2364.
[8] Y. Li, S. Dai, J. John, K.R. Carter, Superhydrophobic surfaces from hierarchically structured wrinkled polymers, ACS Appl. Mater. Interfaces 5 (21) (2013) 11066–11073.
[9] K. Efimenko, J. Finlay, M.E. Callow, J.A. Callow, J. Genzer, Development and testing of hierarchically wrinkled coatings for marine antifouling, ACS Appl. Mater. Interfaces 1 (5) (2009) 1031–1040.
[10] I. Miranda, A. Souza, P. Sousa, J. Ribeiro, E.M. Castanheira, R. Lima, G. Minas, Properties and applications of PDMS for biomedical engineering: A review, J. Funct. Biomater. 13 (1) (2021) 2.
[11] Q. Wang, G. Sun, Q. Tong, W. Yang, W. Hao, Fluorine-free superhydrophobic coatings from polydimethylsiloxane for sustainable chemical engineering: Preparation methods and applications, Chem. Eng. J. 426 (2021) 130829.
[12] C. Yu, K. O'Brien, Y.-H. Zhang, H. Yu, H. Jiang, Tunable optical gratings based on buckled nanoscale thin films on transparent elastomeric substrates, Appl. Phys. Lett. 96 (4) (2010) 041111.
[13] A. Tan, L. Pellegrino, J.A.o.T. Cabral, Tunable phase gratings by wrinkling of plasma-oxidized PDMS: Gradient skins and multiaxial patterns, ACS Appl. Polym. Mater. 3 (10) (2021) 5162–5170.
[14] J.C. McDonald, G.M. Whitesides, Poly (dimethylsiloxane) as a material for fabricating microfluidic devices, Acc. Chem. Res. 35 (7) (2002) 491–499.
[15] M.P. Wolf, G.B. Salieb-Beugelaar, P. Hunziker, PDMS with designer functionalities—Properties, modifications strategies, and applications, Prog. Polym. Sci. 83 (2018) 97–134.
[16] A.K. Singh, et al., Polydimethylsiloxane based sustainable hydrophobic/oleophilic coatings for oil/water separation: A mini review, Cleaner Mater. (2022) 100136.
[17] J.A. Rogers, T. Someya, Y. Huang, Materials and mechanics for stretchable electronics, Science 327 (5973) (2010) 1603–1607.
[18] T. Sathe, D. Bodas, Development and characterization of a polydimethylsiloxane-cellulose acetate hybrid membrane for application in organ-on-a-chip, Mater. Sci. Eng. B 291 (2023) 116366.
[19] M. Nania, F. Foglia, O.K. Matar, J.T. Cabral, Sub-100 nm wrinkling of polydimethylsiloxane by double frontal oxidation, Nanoscale 9 (5) (2017) 2030–2037.
[20] N. Bowden, W.T. Huck, K.E. Paul, G.M. Whitesides, The controlled formation of ordered, sinusoidal structures by plasma oxidation of an elastomeric polymer, Appl. Phys. Lett. 75 (17) (1999) 2557–2559.
[21] W.T. Huck, N. Bowden, P. Onck, T. Pardoen, J.W. Hutchinson, G.M. Whitesides, Ordering of spontaneously formed buckles on planar surfaces, Langmuir 16 (7) (2000) 3497–3501.
[22] D.B. Chua, H. Ng, S.F. Li, Spontaneous formation of complex and ordered structures on oxygen-plasma-treated elastomeric polydimethylsiloxane, Appl. Phys. Lett. 76 (6) (2000) 721–723.
[23] M. Pascual, M. Kerdraon, Q. Rezard, M.-C. Jullien, L. Champougny, Wettability patterning in microfluidic devices using thermally-enhanced hydrophobic recovery of PDMS, Soft Matter 15 (45) (2019) 9253–9260.
[24] X. Tan, D. Rodrigue, A review on porous polymeric membrane preparation. Part II: Production techniques with polyethylene, polydimethylsiloxane, polypropylene, polyimide, and polytetrafluoroethylene, Polymers 11 (8) (2019) 1310.
[25] L. Lin, C.-K. Chung, PDMS microfabrication and design for microfluidics and sustainable energy application, Micromachines 12 (11) (2021) 1350.
[26] R.A. Lawton, C.R. Price, A.F. Runge, W.J. Doherty III, S.S. Saavedra, Air plasma treatment of submicron thick PDMS polymer films: effect of oxidation time and storage conditions, Colloids Surf. A 253 (1–3) (2005) 213–215.
[27] M. Meincken, T. Berhane, P. Mallon, Tracking the hydrophobicity recovery of PDMS compounds using the adhesive force determined by AFM force distance measurements, Polymer 46 (1) (2005) 203–208.
[28] G. Firpo, E. Angeli, L. Repetto, U. Valbusa, Permeability thickness dependence of polydimethylsiloxane (PDMS) membranes, J. Membr. Sci. 481 (2015) 1–8.
[29] A.L. Thangawng, R.S. Ruoff, M.A. Swartz, M.R. Glucksberg, An ultra-thin PDMS membrane as a bio/micro–nano interface: fabrication and characterization, Biomed. Microdev. 9 (4) (2007) 587–595.
[30] D. Neas, P. Klapetek, Gwyddion: an open-source software for SPM data analysis, Central Euro. J. Phys. (ISSN: 1895-1082) 10 (2012) 181–188, http://dx.doi.org/10.2478/s11534-011-0096-2.
[31] K. Tsougeni, A. Tserepi, G. Boulousis, V. Constantoudis, E. Gogolides, Tunable poly(dimethylsiloxane) topography in O2 or Ar plasmas for controlling surface wetting properties and their ageing, Japan. J. Appl. Phys. 46 (2R) (2007) 744.
[32] L. Nunes, Mechanical characterization of hyperelastic polydimethylsiloxane by simple shear test, Mater. Sci. Eng. A 528 (3) (2011) 1799–1804.
[33] Y. Cao, D. Yang, W. Soboyejoy, Nanoindentation method for determining the initial contact and adhesion characteristics of soft polydimethylsiloxane, J. Mater. Res. 20 (8) (2005) 2004–2011.
[34] P. Hermanowicz, M. Sarna, K. Burda, H. Gabryś, AtomicJ: an open source software for analysis of force curves, Rev. Sci. Instrum. 85 (6) (2014) 063703.
[35] F. Rico, P. Roca-Cusachs, N. Gavara, R. Farré, M. Rotger, D. Navajas, Probing mechanical properties of living cells by atomic force microscopy with blunted pyramidal cantilever tips, Phys. Rev. E 72 (2005) 021914, http://dx.doi.org/10.1103/PhysRevE.72.021914, URL https://link.aps.org/doi/10.1103/PhysRevE.72.021914.
[36] M. Strobel, C.S. Lyons, An essay on contact angle measurements, Plasma Process. Polym. 8 (1) (2011) 8–13.
[37] H. Eral, D. t Mannetje, J.M. Oh, Contact angle hysteresis: a review of fundamentals and applications, Colloid Polym. Sci. 291 (2) (2013) 247–260.

[38] Y. Xiang, P. Fulmek, D. Platz, U. Schmid, Temperature dependence of water contact angle on teflon AF1600, Langmuir (2022).
[39] E. Bormashenko, Y. Bormashenko, G. Whyman, R. Pogreb, A. Musin, R. Jager, Z. Barkay, Contact angle hysteresis on polymer substrates established with various experimental techniques, its interpretation, and quantitative characterization, Langmuir 24 (8) (2008) 4020–4025.
[40] C. Bourges-Monnier, M. Shanahan, Influence of evaporation on contact angle, Langmuir 11 (7) (1995) 2820–2829.
[41] J.-B. Valsamis, M. De Volder, P. Lambert, Physical background, in: Surface Tension in Microsystems, Springer, 2013, pp. 3–16.
[42] Y. Xiang, P. Fulmek, D. Platz, U. Schmid, Temperature-dependent electrowetting behavior on teflon AF1600, J. Mater. Sci. 57 (31) (2022) 15151–15159.
[43] E. Delamarche, A. Bernard, H. Schmid, A. Bietsch, B. Michel, H. Biebuyck, Microfluidic networks for chemical patterning of substrates: design and application to bioassays, J. Am. Chem. Soc. 120 (3) (1998) 500–508.
[44] I. Johnston, D. McCluskey, C. Tan, M. Tracey, Mechanical characterization of bulk sylgard 184 for microfluidics and microengineering, J. Micromech. Microeng. 24 (3) (2014) 035017.
[45] M. Inoue, E. Ismail, S. Samitsu, H. Kanoh, I. Ichinose, High hexane sorption capacity of loosely crosslinked PDMS rubbers at low temperatures: Macromolecular and physicochemical elucidation for VOC recovery, Separ. Purif. Technol. (2022) 122634.
[46] S. Béfahy, P. Lipnik, T. Pardoen, C. Nascimento, B. Patris, P. Bertrand, S. Yunus, Thickness and elastic modulus of plasma treated PDMS silica-like surface layer, Langmuir 26 (5) (2010) 3372–3375.
[47] J. Genzer, J. Groenewold, Soft matter with hard skin: From skin wrinkles to templating and material characterization, Soft Matter 2 (4) (2006) 310–323.
[48] H. Jiang, D.-Y. Khang, J. Song, Y. Sun, Y. Huang, J.A. Rogers, Finite deformation mechanics in buckled thin films on compliant supports, Proc. Natl. Acad. Sci. 104 (40) (2007) 15607–15612.
[49] B. Sarrazin, R. Brossard, P. Guenoun, F. Malloggi, Investigation of PDMS based bi-layer elasticity via interpretation of apparent Young's modulus, Soft Matter 12 (7) (2016) 2200–2207.
[50] F.A. Bayley, J.L. Liao, P.N. Stavrinou, A. Chiche, J.T. Cabral, Wavefront kinetics of plasma oxidation of polydimethylsiloxane: limits for sub-μm wrinkling, Soft Matter 10 (8) (2014) 1155–1166.
[51] B.A. Glatz, A. Fery, The influence of plasma treatment on the elasticity of the in situ oxidized gradient layer in PDMS: Towards crack-free wrinkling, Soft Matter 15 (1) (2019) 65–72.
[52] T. Young, III. An essay on the cohesion of fluids, Philos. Trans. R. Soc. Lond. (95) (1805) 65–87.
[53] N. Vargaftik, B. Volkov, L. Voljak, International tables of the surface tension of water, J. Phys. Chem. Ref. Data 12 (3) (1983) 817–820.